Journal of Alloys and Compounds 908 (2022) 164629

Contents lists available at ScienceDirect

Journal of Alloys and Compounds

journal homepage: www.elsevier.com/locate/jalcom

Research Article

Enhanced Atenolol oxidation by ferrites photoanodes grown on ceramic SnO_2-Sb_2O_3 anodes

J. Carrillo-Abad[a,*], J. Mora-Gómez[a], M. García-Gabaldón[a], M.T. Montañés[a], S. Mestre[b], V. Pérez-Herranz[a]

[a] IEC Group, Universitat Politècnica de València, Camí de Vera s/n, 46022 València, Spain
[b] Instituto de Tecnología Cerámica, Campus Universitario Riu Sec, Av.Vicent Sos Baynat s/n, 12006 Castelló, Spain

ARTICLE INFO

Article history:
Received 29 November 2021
Received in revised form 9 March 2022
Accepted 15 March 2022
Available online 16 March 2022

Keywords:
Atenolol
Ceramic electrodes
Electrochemical reactions
Ferrites
Photoanodes

ABSTRACT

The increase in the consumption of pharmaceutical compounds has caused the increment of their presence in different body waters. β-blockers are one of the most dangerous even at low concentrations (ng L^{-1}). Anodic oxidation with a boron-doped diamond (BDD) anode presents good results to remove these compounds. However, since this anode is expensive, some cheaper materials are under study. In this work, Sb-doped SnO_2 ceramic anodes (BCE) coated with Zn or Cd ferrites, in order to provide photocatalytic properties, have been applied to the degradation of the Atenolol (ATL) β-blocker. Increasing the applied current increased ATL degradation and mineralization but caused a decrease in mineralization current efficiency (MCE) and an increase in energy consumption (E_{TOC}). Additionally, light irradiation enhanced the ATL mineralization rate between 10% and 20% for both ferrites, although this increase was higher for the cadmium ferrite one. Finally, when the ferrites were compared with BDD and BCE anodes, the oxidizing power of the different anodic materials can be ordered as follows BDD > Cd-Fe > Zn-Fe > BCE. Therefore, both ferrites improved the BCE performance but only the cadmium one appeared as an alternative to the BDD, especially for MCE and $E_{TOC,}$ reaching values of 15% and 0.5 kWh g_{TOC}^{-1}, respectively.

1. Introduction

The consumption of pharmaceutical compounds is increasing daily by both humans and livestock. Therefore, its presence in surface and ground body waters has become a potential health risk for wildlife and human beings [1,2]. Furthermore, the conventional wastewater treatment is inefficient for the removal of these pharma compounds, which makes them remain in body waters [3]. Among these substances, the β-blockers appear as one of the most dangerous since they are harmful even at low concentrations (ng L^{-1}). Atenolol (ATL) is a widely used β-blocker employed in the treatment of anti-angina, cardiovascular diseases, and hypertension. Only in Europe, the consumption of β-blockers is higher than 3 tons per year. Furthermore, approximately 50% of the administered ATL dose (up to 100 mg per patient per day) is excreted in the urine, with practically 90% of the ATL still intact [3]. As a consequence, ATL is present in groundwater at concentrations up to 10 μg L^{-1} [4]. Locally in Spain, ATL has been detected in the range of 0.84–2.8 μg L^{-1} in some wastewaters [5].

Due to this reason, in the last years, many kinds of research have been focused on the elimination of these emerging compounds [6–11]. Among these studies, the Advanced Oxidation Processes (AOPs) are interesting methods able to remove these substances. The electrochemical advanced oxidation processes (EAOPs) are especially attractive because of their high effectiveness, low cost, and no use of chemicals [12–14]. Between them, anodic oxidation is one of the most prominent techniques. Anodic oxidation is based on the generation of oxidant species, mainly the hydroxyl radical, which are able to completely oxidize organic pollutants to CO_2 and H_2O due to their high oxidizing potentials [15,16]. Although some different materials, like TiO_2/RuO_2, graphene, Ti/PbO_2, etc., are employed as anodes [17–19], boron-doped diamond (BDD) anodes are, nowadays, one of the most efficient electrodes. BDD presents a high reactivity, great O_2 overpotential, and high chemical and thermal stability [20–22]. Nevertheless, this material presents a high cost and difficulty in its manufacture as main drawbacks.

In this work, new ceramic materials capable of competing with BDD are being developed [23–25]. Their main advantages are a great active area, high porosity, low cost and easiness of manufacture. In

* Corresponding author.
E-mail address: jorcarab@upvnet.upv.es (J. Carrillo-Abad).

https://doi.org/10.1016/j.jallcom.2022.164629
0925-8388/

our previous works, a basic ceramic electrode (BCE) composed of SnO_2 doped with Sb_2O_3 has shown its effectiveness to deplete Norfloxacin and ATL from solution [26,27]. However, the results obtained by this BCE were not as good as the ones provided by BDD. In this sense, new photocatalytic materials, based on iron spinel ferrites, deposited on the BCE surface have been tested with the purpose of improving the performance of the ceramic anodes aforementioned. Iron spinel ferrites were selected due to their abundance in the earth, low fabrication cost, non-toxicity, high surface area, porosity, thermal and chemical stability, antimicrobial potential, high activity, narrow bandgap (1.1–2.3 eV), high stability under visible light-irradiation and excellent electrochemical properties [28–32].

Furthermore, simultaneous electrocatalytic and photocatalytic degradation of organic pollutants in wastewaters is generating interest as it could combine direct contact amongst photocatalytic active material and the electrode substrate to ensure a rapid electron transport, full solar spectrum photocatalysis, and high photoelectric conversion efficiency due to many photocatalytic active sites [33]. Moreover, this kind of photoanode avoids the need for the separation of the photocatalyst particles from the effluent since they are fixed on the electrode surface [34,35].

2. Materials and methods

2.1. Reagents and solutions preparation

Both $NaSO_4$ and pure Atenolol employed to make the electrolyte and standard solutions, respectively, were purchased from Sigma-Aldrich. Concerning the ATL used in the experiments, it was obtained from Atenolol NORMON 100 mg© pharmaceutical pills. To extract the ATL present in the pills, they were mashed and solved into distilled water, after the pH was set to 3 adding H_2SO_4. Then, the solution was maintained under stirring conditions for 1 h to completely dissolve the ATL present in the pills. Finally, the resulting solution was filtered with 57 µm fiberglass filters to eliminate excipients.

2.2. Electrode fabrication and coating

The synthesis and processing of the basic ceramic electrodes (BCE) were well described in previous works elsewhere [36]. Both ferrite powders were synthesized by the solution combustion synthesis process that was already employed for spinel-type pigments [37,38]. A mixture of iron nitrate and Cd or Zn nitrate were dissolved in distilled water under stirring conditions. Afterward, urea was added to the sample as fuel. The combustion took place in a kiln preheated at 500 °C (BLF 1800, Carbolite Furnaces Ltd, UK) for 20 min to assure the complete combustion reaction. This process was tripled and the resulting powders mixed to reduce the variability of the method. Samples of these ferrite powders were mixed with SnO_2 (40/60 in wt%) and calcined at 1100 °C for 1 h in an electric furnace (RHF 1600, Carbolite Furnaces Ltd, UK) in order to detect possible interactions amongst the catalyst and the substrate.

The suspension employed for dip-coating the BCE consisted of a mixture of the selected ferrite and IsM (1/99 wt%). This suspension was milled in a planetary mill with micro balls (Pulverisette 5, Fritsch GmbH, Germany) for 60 min at 260 rpm. Then, the suspension was diluted to 0.6 wt% in ferrite with IsM to produce a high-quality layer on the electrode surface. The dip-coating of the catalyst was performed in a homemade apparatus, which permits the control of immersion and emersion times and speeds. Afterward, the resulting electrodes were dried in an oven that fixed the catalyst thermally. This treatment consisted of heating at 10 ºC min^{-1} up to 1100 ºC and 1 h of soaking time, in an electric furnace (RHF 1400, Carbolite Furnaces Ltd. UK). During the soaking time, the sample dries, foam, boils, ignites, and burns to achieve temperatures up to 1500 °C [39].

2.3. Electrode characterization

The Archimedes method was employed to determine the density of the sintered electrodes. The electrical resistivity of the sintered samples was measured by a four points method with HIOKI RM3545 equipment (Hioki E.E. Corporation, Japan), in a homemade setup. An X-ray diffractometer (Theta-Theta D8 Advance, Bruker, Germany) was used for the characterization of crystalline structures. The radiation was based on CuK with a λ = 1.54183 Å. A lamp of 45 kV using 40 mA of intensity light was employed. A VÅNTEC-1 detector in a 2θ from 5° to 90° with a step width of 0.015° and a counting time of 1.2 s/step was employed to obtain the XRD data.

2.4. Photo-electrolysis experiments

A Pyrex glass of 250 mL was employed as a photo-electrochemical reactor. The solution employed in the experiments contained 100 mg L^{-1} of ATL in 2 g L^{-1} Na_2SO_4. In all the experiments, an AISI 304 stainless steel sheet with an exposed area of 20 cm^2 was used as a cathode. The anodic materials employed were, the BDD, the BCE, and the ferrites electrodes. These ferrites were obtained by the dip-coating method aforementioned of the BCE in the Zn or Cd ferrite powder, and named as Zn-Fe and Cd-Fe, respectively. The contact surface of the anode was 12 cm^2. To provide the light irradiation, a 150 W (high-pressure Hg) VIS-light lamp was utilized, whose main photon peaks are in the 300–600 nm region. The position of the lamp allowed a 15º inclination of the irradiated light. The temperature of the experiments was maintained at 30ºC, and they were under stirring conditions. Fig. 1 represents a diagram of the experimental setup together with a picture of both ferrite anodes.

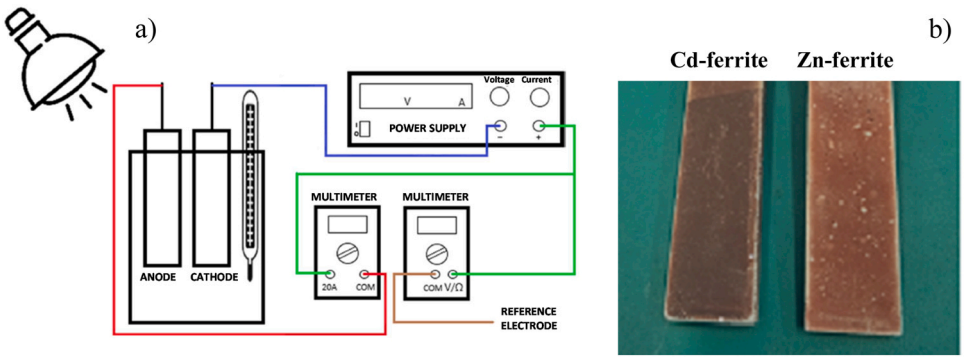

Fig. 1. Diagram of the experimental setup, a), picture of the ferrite anodes b).

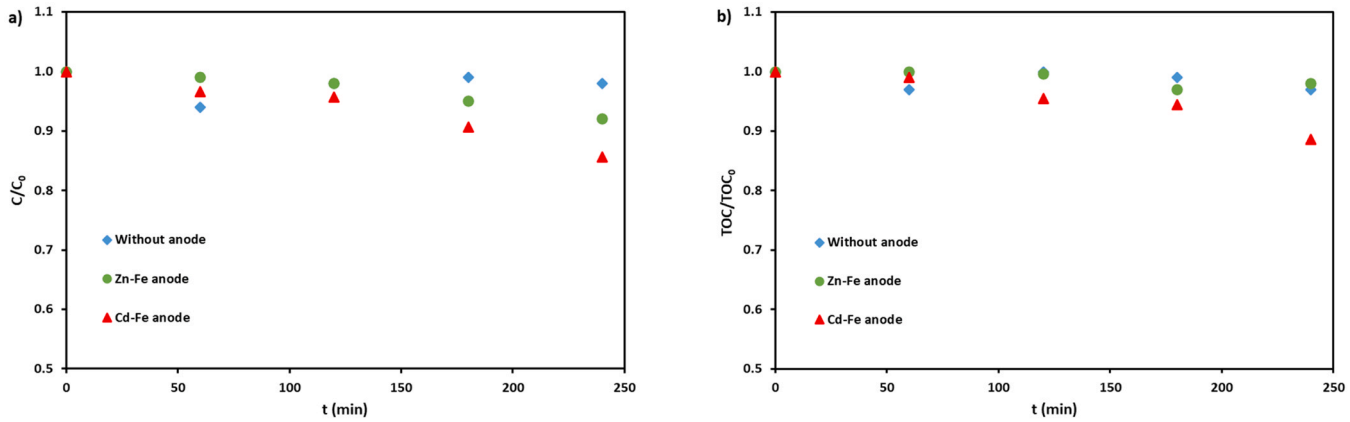

Fig. 2. ATL, a), and TOC, b), relative concentration evolution with time without any applied current in the absence of anodes and in the presence of both ferrites.

The applied current ranged from 0 to 66.67 mA cm^{-2}. Experiments without applied current were performed to determine the stability of ATL under VIS-light irradiation and the photocatalytic behavior of the Zn and Cd ferrites. In these experiments, a multimeter was employed to record the current values generated by the anode under light irradiation. The current values were controlled using a power supply. Both current and cell voltage were recorded during the experiments. Samples were taken from the reactor every 15 min during the first hour and each 30 min thereafter.

After each experiment, the final dissolution was analyzed by atomic absorption spectroscopy (AAS) using a Perkin-Elmer model Analyst 100 with a Cadmium hollow cathode lamp at 228.8 nm wavelength, 0.7 nm spectral bandwidth, and an operating current of 5 mA.

2.4.1. Analysis of Atenolol oxidation and mineralization

The evolution of ATL concentration was monitored by a high-performance liquid chromatograph (HPLC). The HPLC system had a Kinetex XB-C18 column (100×4.6 mm, 5 µm, 100 Å), a PU-2089 quaternary gradient pump (Jasco, Japan), and a Photodiode Array detector MD2018 Plus. The applied conditions were: injected volume of 20.0 µL, a flow rate of 1 mL min^{-1}, and a wavelength-UV detection at 224 nm. A mobile phase based on an isocratically methanol-water 15:85 (v/v) mixture was used.

Concerning the total organic carbon (TOC), it served to calculate the ratio of mineralization achieved during the ELOX process. To measure this parameter a Shimadzu TNM-L ROHS TOC analyzer was employed. The working method was the non-purgeable organic carbon (NPOC), where inorganic C is depleted by HCl addition prior to measuring the TOC concentration.

2.4.2. Anode performance

Once measured ATL and TOC concentrations, the extent of electrochemical combustion (Φ) [40,41] was calculated as:

$$\Phi = \frac{\%[TOC]_{removed}}{\%[ATL]_{removed}} \quad (1)$$

Φ range from 0 to 1, where 0 indicates a process with degradation but without combustion while 1 implies complete mineralization of all the previously oxidized ATL.

Another parameter to analyse the electrode performance is the mineralization current efficiency (MCE). It is defined as the ratio between the amount of current used in mineralizing the organic carbon and the total applied current. Its equation for a given time t, in min, is [42,43]:

$$MCE(\%) = \frac{n\,F\,V\,\Delta[TOC]_t}{7.2 \cdot 10^5 m\,I\,t}\,100 \quad (2)$$

where $\Delta[TOC]_t$ (mg L^{-1}) is the TOC removal after the given time, F is the Faraday constant (96485 C mol^{-1}), n implies the number of electrons exchanged during the oxidation reaction, V means the reactor volume (L), m represents the number of C atoms in the ATL molecule (14), I is the applied current (A) and $7.2{\cdot}10^5$ is a conversion factor (60 s min^{-1} x 12,000 mg mol^{-1}). n was determined from Eq. (3), where the mineralization of ATL is shown considering that all the molecular nitrogen forms ammonium ions. This assumption was corroborated in previous studies [27,44].

$$C_{14}H_{22}N_2O_3 + 25H_20 \rightarrow 14CO_2 + 2NH_4^+ + 64H^+ + 66e^- \quad (3)$$

Finally, the energy consumption per mass of TOC eliminated E_{TOC} (kWh mg_{TOC}^{-1}) is a useful parameter to compare this process with others in an economical way. It is worth to notice that the energy spent by the lamp is not counted, since this work wants to emulate the use of sunlight. Eq. (4) was used to determine E_{TOC} [45,46]:

$$E_{TOC} = \frac{\int_0^t U(t)\,I \quad dt}{\Delta[TOC]_t\,V} \quad (4)$$

where U is the cell voltage (V).

3. Results and discussion

3.1. Atenolol stability and photocatalytic activity of ferrites

Fig. 2 represents the ATL and TOC relative concentrations for the experiments performed without applying any current but under VIS-light irradiation, that is, ATL solution without any electrode, ATL with Zn-ferrite, or with Cd-ferrite. From these experiments, the following conclusions could be deduced, firstly, ATL appears as a good probe molecule as it is not degraded neither mineralized by the VIS-light irradiation. Secondly, both Zn and Cd ferrites exhibited photocatalytic activity as they caused a slight decrease in both ATL and TOC relative concentrations. Furthermore, both ferrites registered current between the electrodes caused by the light irradiation, from 15 to 30 and 25–50 mA for Zn and Cd ferrite, respectively, which corroborates that they are acting as photoanodes. Comparing both ferrites, Cd-ferrite shows a higher degradation and mineralization degree than Zn ferrite. In the literature, some authors have also demonstrated the photocatalytic activity of Zn-Fe [47–49] and Cd-Fe [50–52] for environmental applications and hydrogen generation.

3.2. Current effect on ferrite behavior

Fig. 3a) and b) depict ATL and TOC relative concentration evolution for Zn-Fe ferrite. For a given instant time both parameters decrease with the applied current. Additionally, ATL degradation

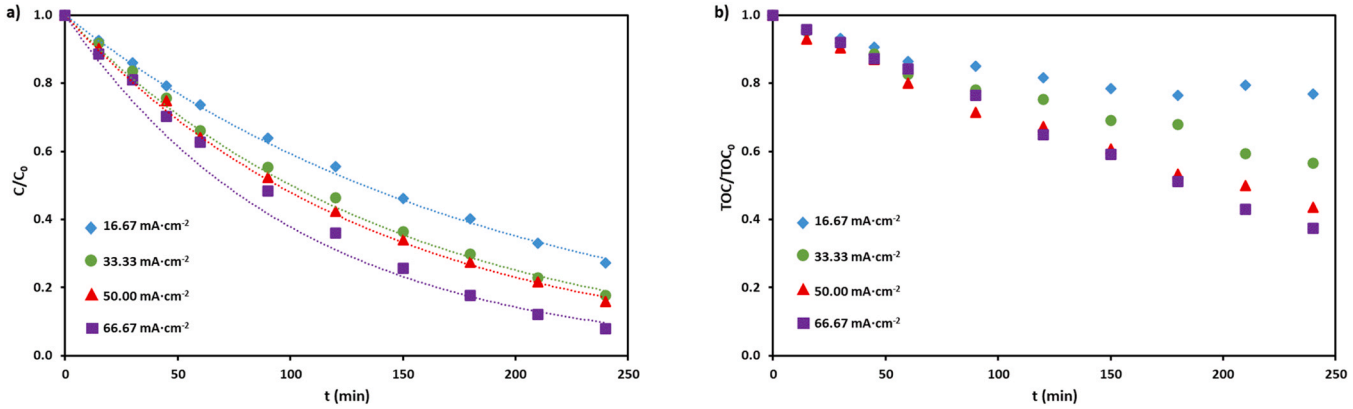

Fig. 3. ATL, a), and TOC, b), relative concentration evolution with time for the Zn-Fe anode under all the applied current values. The theoretical ATL decay is represented by the continuous lines.

Table 1
Pseudo-first order kinetic constants (k')·10^{-3} (min^{-1}) as a function of the applied current density.

i (mA/cm^2)	16.67	33.33	50.00	66.67
Zn-Fe	5.23	6.91	7.34	9.72
Cd-Fe	5.47	7.07	8.66	10.54

shows a pseudo-first-order kinetic that is associated with an indirect oxidation process controlled by ATL mass transfer from the bulk solution to the anode interface, where it reacts with the •OH generated. This behavior was previously observed for the BCE anode without ferrite coating [27]. Consequently, increasing the applied current density caused an increase in ATL degradation and in its mineralization due to the •OH concentration increase with the applied current density [20]. This fact is corroborated with the values of the pseudo-first-order kinetic constant (k') determined for ATL degradation, which is presented in Table 1. Moreover, the continuous lines presented in Fig. 3a), which represent ATL relative concentration calculated by the values of k', correctly fit the experimental data, which verifies the control of ATL degradation by mass transfer.

It is worth to note that, initially, the TOC decay (Fig. 3b)) presents similar values for all the applied current up to 60 min of electrolysis. This suggests that •OH radicals mainly attack ATL until a high number of intermediates are present in solution, whose further

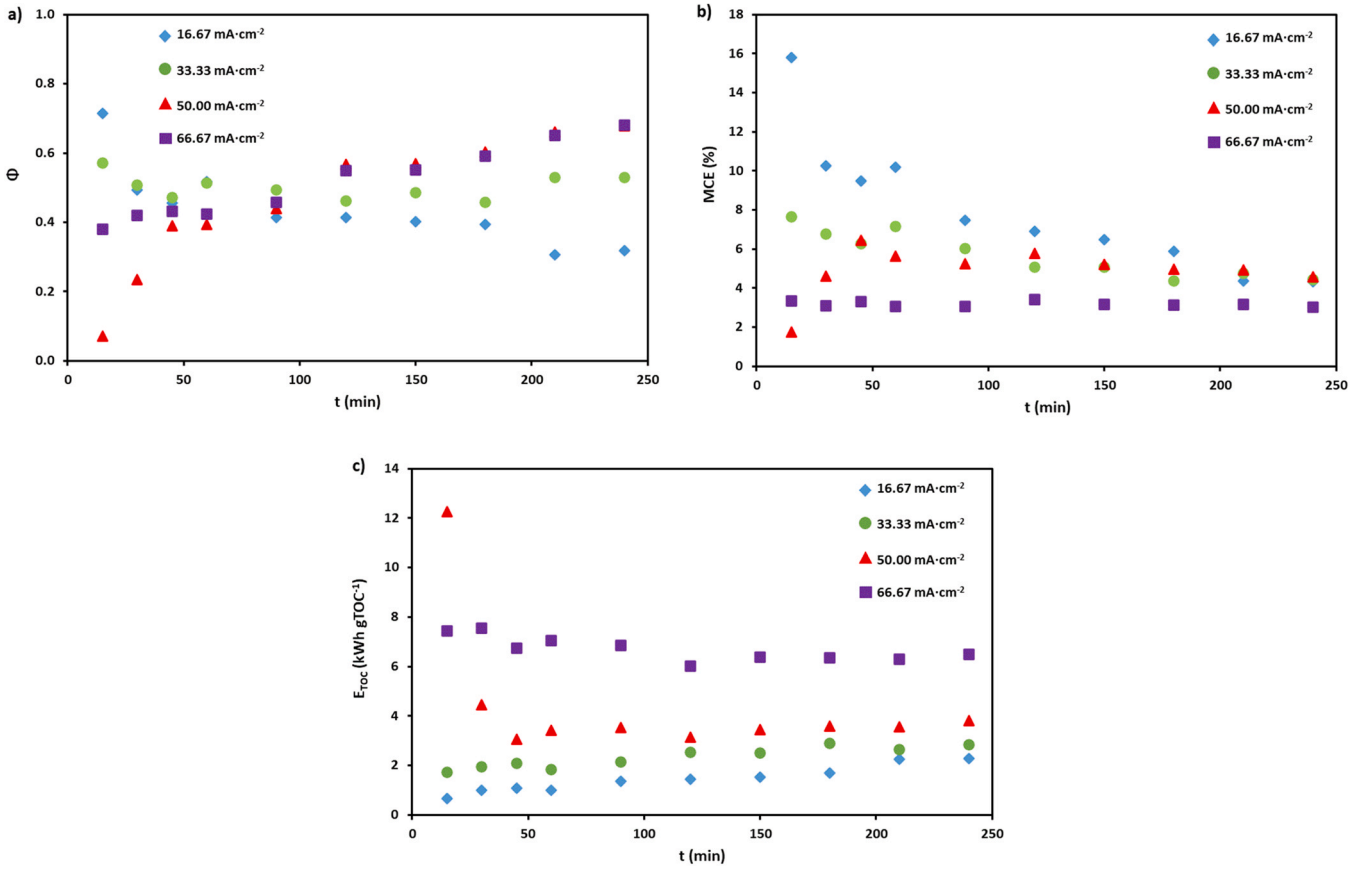

Fig. 4. Evolution with time of electrochemical combustion extent, a), MCE, b), and energy consumption per gram of TOC depleted, c), for the Zn-Fe anode under all the applied current values.

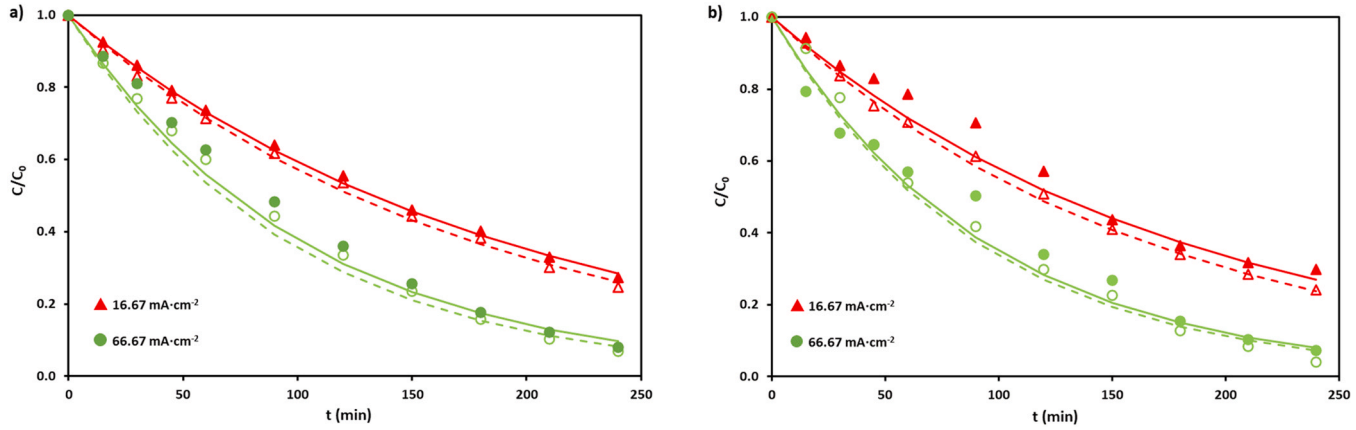

Fig. 5. ATL relative concentration decay for Zn-Fe, a), and Cd-Fe, b) anodes for 16.67 and 66.67 mA cm^{-2} under dark (full points) and light conditions (empty points). Theoretical ATL decay is represented by the continuous lines.

Table 2
Pseudo first order kinetic constants (k′)·10^{-3} (min^{-1}) obtained for both ferrites at light and dark conditions.

i (mA/cm^2)	16.67		66.67	
Conditions	*Dark*	*Light*	*Dark*	*Light*
Zn-Fe	5.23	5.59	9.72	10.40
Cd-Fe	5.47	5.97	10.54	10.94

oxidation conducts to the complete mineralization. The final relative concentration of both ATL and TOC were 0.272 and 0.768, 0.177 and 0.565, 0.160 and 0.436, 0.079 and 0.373 for 16.67, 33.33, 50.00 and 66.67 mA cm^{-2}, respectively.

Regarding the Cd-Fe anode (not shown), the same conclusions about the applied current effect on the anode performance were obtained, but in this case, the final values of ATL and TOC relative concentrations were 0.297 and 0.542, 0.165 and 0.481, 0.121 and 0.366, 0.072 and 0.306 for the aforementioned applied currents. Hence, the Cd-ferrite anode presents a higher oxidizing power than Zn-Fe one. On the other hand, the same determining step was observed (mass transfer control) and the pseudo-first kinetic constant were determined and also appears in Table 1. Comparing the k′ values for both ferrites, independently of the current applied, it is observed that the Cd-Fe anode presented higher values. The best performance of the Cd-Fe anode may be related to the oxidizing power of the Cd(I)/Cd(II) redox couple.

Fig. 4 shows the evolution of the electrochemical extent, a), the mineralization current efficiency, b), and the energy consumption per gram of TOC depleted for the Zn-Fe anode under all the applied current values. Concerning the electrochemical extent, increasing the applied current caused an increase in this parameter since a higher amount of the ATL degraded could also be mineralized. Regarding the MCE, the higher the applied current the lower the MCE is as more ˙OH radicals were generated, which increased the chance of side reactions, such as the electrolyte oxidation or the hydroxyl radical recombination [20]. It is worth noting that 50.00 mA cm^{-2} did not show this decrease, which could mean an increase in the mass transfer that permits the ˙OH to react with the organic matter. Finally, an increase in the applied current value caused an increase in the energy consumption due to the higher importance of the parasitic reactions, as mentioned above for the MCE. For this last parameter, the phenomenon observed in the MCE for 50.00 mA cm^{-2} is not shown maybe because the increase in the cell potential was higher than the mass transfer promoting effect. In regard to the Cd-Fe anode, not shown, its behavior was similar to that observed for the Zn-Fe although the MCE was slightly higher and the energy consumption a little lower for this anode compared to the Zn-Fe one. These results are related to the higher oxidizing power of the Cd-Fe anode.

3.3. Photo-electrooxidation experiments

Once determined the effect of modifying the applied current density on the anode performance and corroborated the photoactivity of both anodes, the effect of light irradiation on the anode's performance during the electro-oxidation experiments is analysed. Fig. 5 represents the evolution of ATL degradation under dark and light conditions for Zn-Fe, a), and Cd-Fe, b) anodes for the lowest and

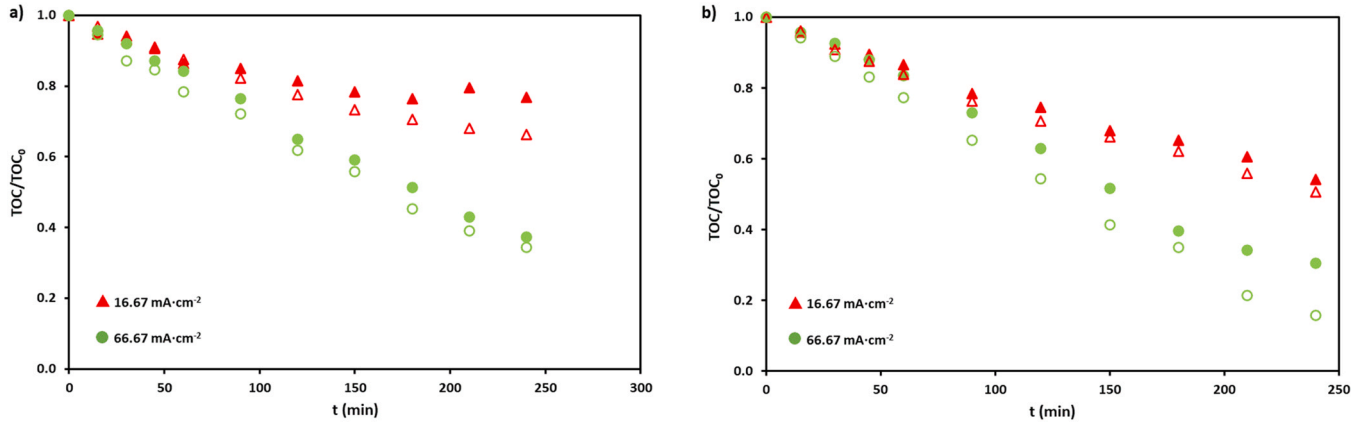

Fig. 6. TOC relative concentration decay for Zn-Fe, a), and Cd-Fe, b), anodes for 16.67 and 66.67 mA cm^{-2} under dark (full points) and light conditions (empty points).

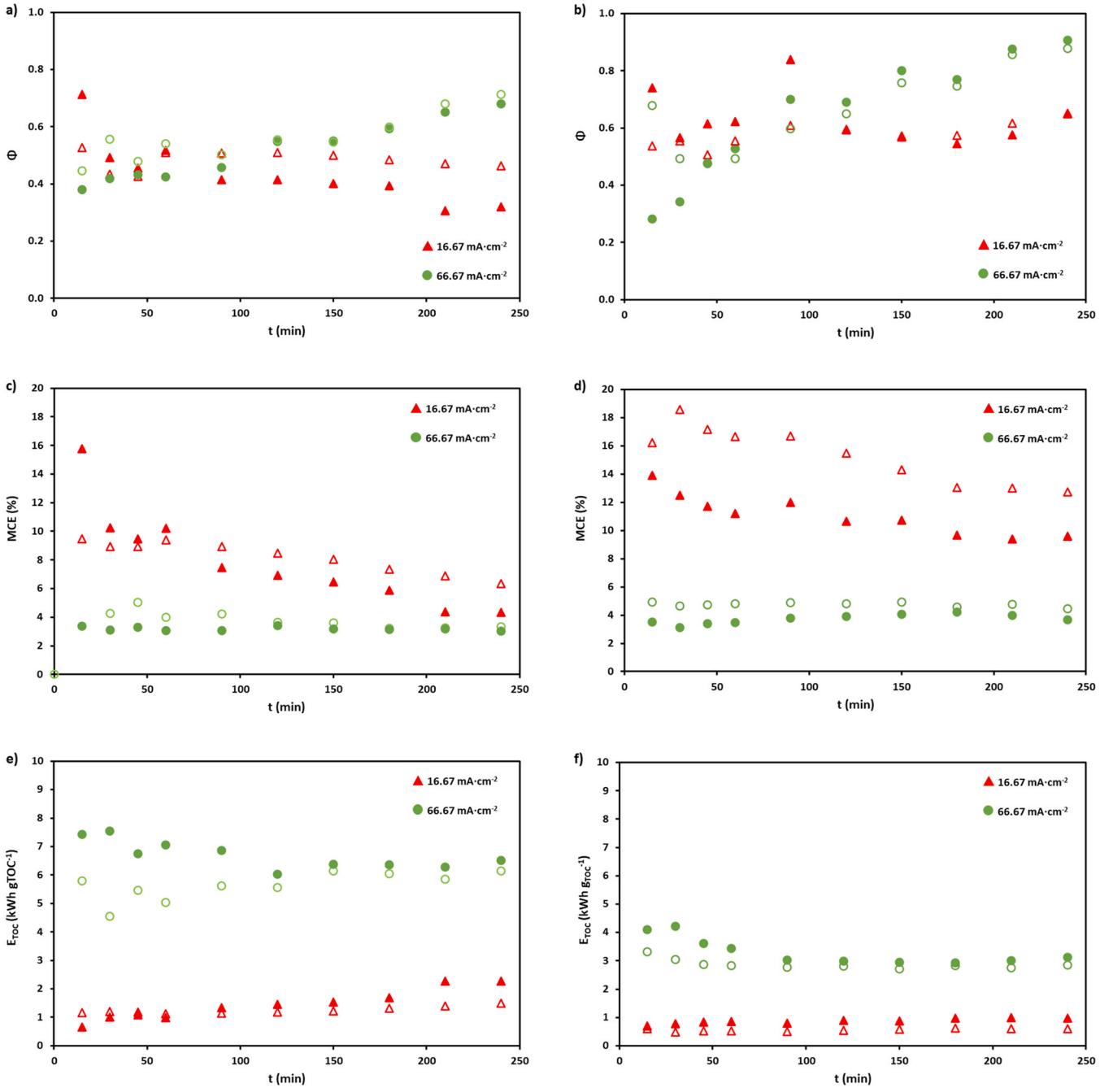

Fig. 7. Evolution of the electrochemical extent, MCE and energy consumption per gram of TOC depleted for Zn-Fe, a), c), e), and Cd-Fe, b), d), f) anodes for 16.67 and 66.67 mA cm^{-2} under dark (full points) and light conditions (empty points).

highest applied current values. A slight increase in ATL degradation is observed under light irradiation, especially at 16.67 mA cm^{-2}. Furthermore, it can be concluded that visible light irradiation does not modify the limitation step, that is, the ATL mass transfer from bulk solution to the anode vicinity. Comparing the values of the apparent kinetic constants of both ferrites, which appear at Table 2, it can be concluded that applying visible light radiation to both anodes causes an increase in their degradation rate, which is associated with a higher amount of oxidant species generated at the anode due to their photo-electrocatalytic activity. Moreover, the Cd-Fe presents higher kinetic constant under both dark and light conditions.

Furthermore, comparing the TOC decay of both ferrites under light and dark conditions, Fig. 6a) and b), it is noted that the Cd-Fe anode presented a higher mineralization power under both light and dark conditions. Specifically, the increment in the TOC depletion is more remarkable than that observed for ATL degradation for light conditions. For example, Zn ferrite achieved a 23% and 62% of mineralization for 16.67 and 66.67 mA cm^2 at dark conditions while these values increased to 34% and 66% at light conditions. On the other hand, Cd ferrite presented 45% and 69% of mineralization for 16.67 and 66.67 mA cm^2 at dark conditions. These values increased to 50% and 84% under light irradiation. The better performance of the Cd-Fe anode could be associated with the participation of the redox pair Cd(I)/Cd(II) together with the higher structural defects of this ferrite [53–55] since both ferrites present the same base material and, consequently, approximately the same specific surface. Specifically, the better performance observed under light conditions

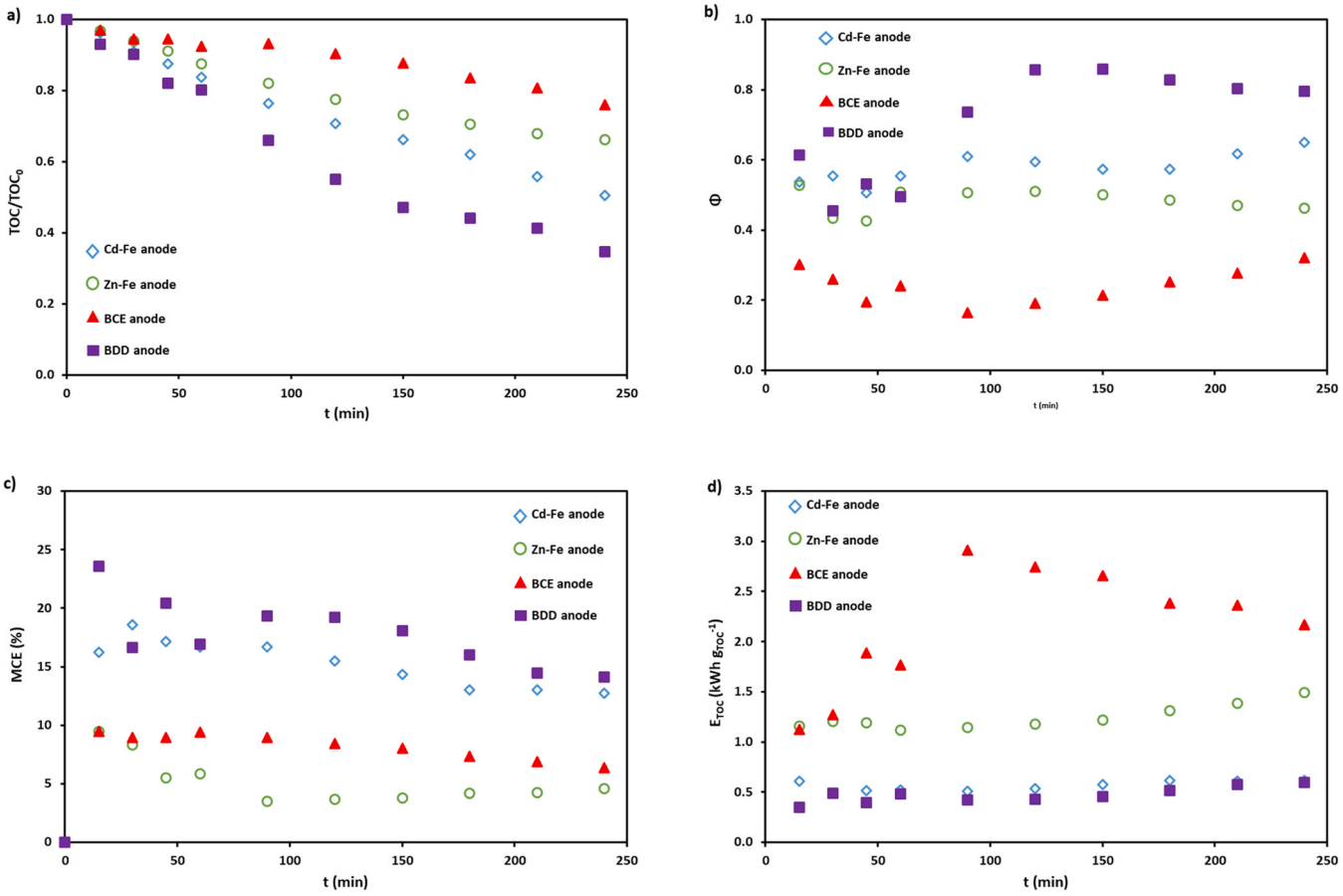

Fig. 8. Evolution of TOC relative concentration a), electrochemical extent, b), MCE, c) and E_{TOC}, d), for Cd-Fe, Zn-Fe, BCE, and BDD anodes for 16.67 mA cm^{-2} under dark (full points) and light conditions (empty points).

could be related to cadmium presence, which could generate the unstable cation Cd(I) [56,57]. This unstable redox state could help during the ELOX process, generating oxidizing species or degrading some organic matter.

For both ferrites, the evolution of the electrochemical extent, MCE and energy consumption per gram of TOC depleted with time is analogue as that shown in Fig. 7. This means that increasing the applied current improved the electrochemical extent but worsened both MCE and the energy consumption, which follows the typical behaviour of an electrochemical reactor [26,27,58,59]. This behaviour is related to the increase in the generation of oxidizing species that increase the mineralization rate more than the ATL degradation, but it also increases side reactions. Furthermore, analysing the light irradiation effect on the anode performance, a slight enhance was observed for the Zn-Fe while a higher improvement effect was obtained for the Cd-Fe, where MCE higher than 15% was achieved at 16.67 mA cm^{-2}. These results are in concordance with the previous photocatalytic experiments, where the Cd-Fe presented better results when only light irradiation was applied.

3.4. Anodic material comparison

Once was corroborated that light irradiation enhanced ferrites' performance, these materials were compared with the basic ceramic electrode without coating, BCE, and with a commercial boron-doped diamond electrode, BDD. Fig. 8a) depicts TOC relative concentration evolution with time for all the materials tested under 16.67 mA/cm^{-2}. As BDD and BCE are non-photoactive anodes, their results were only obtained in dark conditions. Although BDD shows a slightly better behavior in terms of ATL degradation, all the anodes presented good results, achieving practically the 80% of ATL degradation at the end of the experiments (not shown). However, concerning the TOC decay, the results obtained considerably differs from one anode to another. In this case, the mineralization power of the anodes increased in the order of: BCE < Zn-Fe < Cd-Fe < BDD, which were able to achieve a 25%, 34%, 50% and 66% of mineralization degree, respectively.

The evolution of the electrochemical extent is depicted in Fig. 8b). As the degradation rate was very similar for all the anodes studied, the mineralization degree caused practically all the differences observed of this parameter. Consequently, the BDD anode presented the highest values, achieving the mineralization up to the 85% of the ATL previously degraded while BCE only achieved the mineralization of the 30% of the oxidised ATL.

The energetic parameters, MCE and energy consumption, Fig. 8c) and d), can also be explained in terms of the mineralization power, that is, the higher mineralization power, the higher MCE and the lower E_{TOC}. Therefore, the BDD appears as the best anode with the lower energy consumption and the highest mineralization current efficiency. However, it is worth to note that the Cd-Fe anode presented MCE differences of only 2% (in average) and also the E_{TOC} values were very similar to those obtained by the BDD.

In summary, comparing the BCE with any of the ferrites under study, both ferrites provided better results for all the parameters studied, which makes the coating of the BCE with these photocatalytic materials an improvement of the SnO_2-Sb_2O_3 anode. As mentioned by [31], $ZnFe_2O_4$ presents some bottlenecks like low charge separation efficiency, low absorption efficiency, etc. Additionally, $CdFe_2O_4$ possesses a more amorphous structure than $ZnFe_2O_4$, which is related to a higher rate of active sites [48]. These

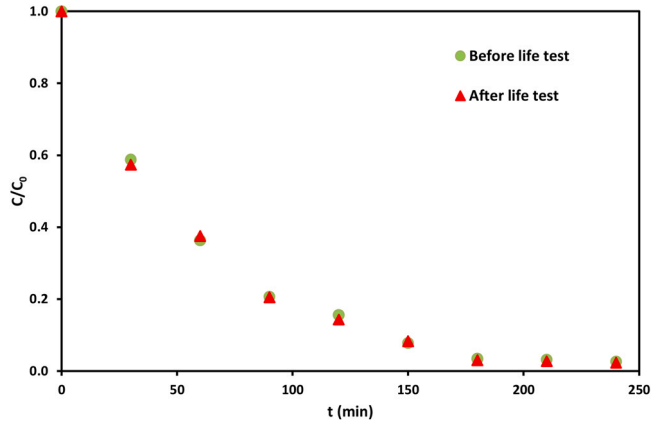

Fig. 9. Evolution of ATL relative concentration decay before (BLT) and after (ALT) the accelerated life test for the Cd-Fe anode and for 114 mA cm^{-2}.

facts could explain the better performance of the Cd-Fe anode over the Zn-Fe one. Finally, although the BDD still exhibits the best anodic performance, the results obtained with the Cd-Fe anode are close enough to represent an alternative to this commercial material.

3.5. Anode stability

The stability of these ceramic electrodes was well established in previous works where a current density of 100 mA cm^{-2} was applied during 70 days on a 0.5 M H_2SO_4 solution [27]. Furthermore, an electro-oxidation experiment was carried out before and after the life test, BLT and ALT respectively, at high current density (114 mA cm^{-2}) to study the effect of the accelerated life test on the oxidizing power of the ceramic electrodes. Fig. 9 shows the evolution of ATL relative concentration with time at this high current value before and after the accelerated life test for the Cd-Fe anode. As observed, there were no significant changes amongst both experiments which means that this material is stable under the experimental conditions tested. The results obtained for the Zn-Fe anode (not shown) were very similar to those observed in Fig. 9. These results are in concordance with other works that previously studied the stability of these materials under oxidation conditions [28–32].

Additionally, due to the toxicity of cadmium, after each electro-oxidation experiment using the Cd-ferrite anode, the final solution was analyzed by AAS to detect Cd presence, which could be released by the electrode oxidation. No Cd was detected at any experiment independently of the applied current value or the light conditions, which suggests that the Cd-ferrite coating is safe enough.

4. Conclusions

The ferrites studied in this work are based on iron oxide doped with another metal (zinc or cadmium) employed to enhance the photocatalytic properties of hematite. Zinc and cadmium ferrites were deposited on a ceramic substrate based on tin oxide doped with antimony with the aim of improving the performance of this ceramic electrode.

Both Cd-Fe and Zn-Fe anodes showed photocatalytic activity, being able of degrading and mineralize Atenolol. It was corroborated that visible light enhanced the performance of both ferrites, although this effect was more remarkable for the TOC decay. Cd-Fe anode presented a better performance under both light and dark conditions, which may be related to the possible generation of the unstable Cd (I) and the higher presence of defects in the Cd-Fe anode.

From the comparison of both ferrites with a commercial BDD and with the basic ceramic electrode that acted as substrate for the ferrites (BCE), it was inferred that BDD showed the best performance, especially in terms of mineralization. The mineralization power of all the anodes under study can be ordered as follows: BDD > Cd-Fe > Zn-Fe > BCE. However, the obtained results with the Cd-Fe anode regarding with the mineralization current efficiency and the energy consumption were close enough to those obtained with the BDD, hence, the cadmium ferrite may represent an alternative to this commercial BDD material, whose manufacture is more difficult and expensive.

CRediT authorship contribution statement

J. Carrillo-Abad: Conceptualization, Validation, Formal analysis, Writing – original draft, Visualization. **J. Mora-Gómez**: Conceptualization, Methodology, Investigation, Writing – review & editing. **M. García-Gabaldón**: Conceptualization, Resources, Writing – review & editing, Supervision. **M.T. Montañés**: Conceptualization, Supervision. **S. Mestre**: Resources, Project administration, Funding acquisition. **V. Pérez-Herranz**: Conceptualization, Resources, Writing – review & editing, Supervision, Project administration, Funding acquisition.

Declaration of Competing Interest

The authors declare that they have no known competing financial interests or personal relationships that could have appeared to influence the work reported in this paper.

Acknowledgments

The authors want to show their gratitude to the Ministerio de Economía y Competitividad (Spain) and the Fondo Europeo de Desarrollo Regional (FEDER) funds that financially support the project RTI2018-101341-B-C21.

References

[1] B. Halling-Sørensen, S. Nors Nielsen, P.F. Lanzky, F. Ingerslev, H.C. Holten Lützhøft, S.E. Jørgensen, Occurrence, fate and effects of pharmaceutical substances in the environment- a review, Chemosphere 36 (1998) 357–393, https://doi.org/10.1016/S0045-6535(97)00354-8
[2] M. al Aukidy, P. Verlicchi, A. Jelic, M. Petrovic, D. Barcelò, Monitoring release of pharmaceutical compounds: occurrence and environmental risk assessment of two WWTP effluents and their receiving bodies in the Po valley, Italy, Sci. Total Environ. 438 (2012) 15–25, https://doi.org/10.1016/J.SCITOTENV.2012.08.061
[3] N. Vieno, T. Tuhkanen, L. Kronberg, Elimination of pharmaceuticals in sewage treatment plants in Finland, Water Res. 41 (2007) 1001–1012, https://doi.org/10.1016/j.watres.2006.12.017
[4] M. Maurer, B.I. Escher, P. Richle, C. Schaffner, A.C. Alder, Elimination of β-blockers in sewage treatment plants, Water Res. 41 (2007) 1614–1622, https://doi.org/10.1016/J.WATRES.2007.01.004
[5] J. Radjenović, M. Petrović, D. Barceló, Fate and distribution of pharmaceuticals in wastewater and sewage sludge of the conventional activated sludge (CAS) and advanced membrane bioreactor (MBR) treatment, Water Res. 43 (2009) 831–841, https://doi.org/10.1016/j.watres.2008.11.043
[6] A. Ponkshe, P. Thakur, Significant mineralization of beta blockers Propranolol and Atenolol by TiO_2 induced photocatalysis, (2019). ⟨www.sciencedirect.comwww.materialstoday.com/proceedings⟩.
[7] A. Özcan, A. Atılır Özcan, Y. Demirci, Evaluation of mineralization kinetics and pathway of norfloxacin removal from water by electro-Fenton treatment, Chem. Eng. J. 304 (2016) 518–526, https://doi.org/10.1016/j.cej.2016.06.105
[8] W. Chen, X. Li, Z. Pan, S. Ma, L. Li, Synthesis of MnOx/SBA-15 for Norfloxacin degradation by catalytic ozonation, Sep. Purif. Technol. 173 (2017) 99–104, https://doi.org/10.1016/j.seppur.2016.09.030
[9] A. Rossner, S.A. Snyder, D.R.U. Knappe, Removal of emerging contaminants of concern by alternative adsorbents, Water Res. 43 (2009) 3787–3796, https://doi.org/10.1016/j.watres.2009.06.009
[10] X. Liu, T. Zhang, Y. Zhou, L. Fang, Y. Shao, Degradation of atenolol by UV/peroxymonosulfate: kinetics, effect of operational parameters and mechanism, Chemosphere 93 (2013) 2717–2724, https://doi.org/10.1016/j.chemosphere.2013.08.090

[11] B. Nicolaisen, Developments in membrane technology for water treatment, Desalination 153 (2003) 355–360, https://doi.org/10.1016/S0011-9164(02)01127-X

[12] J.R. Domínguez, T. González, P. Palo, J. Sánchez-Martín, M.A. Rodrigo, C. Sáez, Electrochemical degradation of a real pharmaceutical effluent, Water Air Soil Pollut. 223 (2012) 2685–2694, https://doi.org/10.1007/s11270-011-1059-3

[13] C.A. Martínez-Huitle, M.A. Rodrigo, I. Sirés, O. Scialdone, Single and coupled electrochemical processes and reactors for the abatement of organic water pollutants: a critical review, Chem. Rev. 115 (2015) 13362–13407, https://doi.org/10.1021/acs.chemrev.5b00361

[14] S. Garcia-Segura, J.D. Ocon, M.N. Chong, Electrochemical oxidation remediation of real wastewater effluents — a review, Process Saf. Environ. Prot. 113 (2018) 48–67, https://doi.org/10.1016/j.psep.2017.09.014

[15] A. Kapałka, G. Fóti, C. Comninellis, The importance of electrode material in environmental electrochemistry. Formation and reactivity of free hydroxyl radicals on boron-doped diamond electrodes, Electrochim. Acta 54 (2009) 2018–2023, https://doi.org/10.1016/j.electacta.2008.06.045

[16] A.R.F. Pipi, I. Sirés, A.R. de Andrade, E. Brillas, Application of electrochemical advanced oxidation processes to the mineralization of the herbicide diuron, Chemosphere 109 (2014) 49–55, https://doi.org/10.1016/j.chemosphere.2014.03.006

[17] S.D. Jojoa-Sierra, J. Silva-Agredo, E. Herrera-Calderon, R.A. Torres-Palma, Elimination of the antibiotic norfloxacin in municipal wastewater, urine and seawater by electrochemical oxidation on IrO_2 anodes, Sci. Total Environ. 575 (2017) 1228–1238, https://doi.org/10.1016/j.scitotenv.2016.09.201

[18] B. Seger, P. v Kamat, Electrocatalytically active graphene-platinum nanocomposites. Role of 2-D carbon support in PEM fuel cells, (2009), 7990–7995. ⟨http://dx.doi.org/10.1021/jp900360k⟩.

[19] P. Cañizares, J. Garcia-Gomez, J. Lobato, M. a Rodrigo, P. Canizares, J. Garcia-Gomez, J. Lobato, M. a Rodrigo, P. Cañizares, J. Garcia-Gomez, J. Lobato, M. a Rodrigo, Modeling of wastewater electro-oxidation processes part II. Application to active electrodes, Ind. Eng. Chem. Res. 43 (2004) 1923–1931, https://doi.org/10.1021/ie0341303

[20] C, G.C. Comninellis, Electrochemistry for the Environment, Springer New York, New York, 2010, https://doi.org/10.1007/978-0-387-68318-8

[21] T.A. Enache, A.M. Chiorcea-Paquim, O. Fatibello-Filho, A.M. Oliveira-Brett, Hydroxyl radicals electrochemically generated in situ on a boron-doped diamond electrode, Electrochem. Commun. 11 (2009) 1342–1345, https://doi.org/10.1016/j.elecom.2009.04.017

[22] J. Carrillo-Abad, V. Pérez-Herranz, A. Urtiaga, Electrochemical oxidation of 6:2 fluorotelomer sulfonic acid (6:2 FTSA) on BDD: electrode characterization and mechanistic investigation, J. Appl. Electrochem. 48 (2018), https://doi.org/10.1007/s10800-018-1180-8

[23] D. Bejan, E. Guinea, N.J. Bunce, On the nature of the hydroxyl radicals produced at the boron-doped diamond and Ebonex ® anodes, Electrochim. Acta 69 (2012) 275–281, https://doi.org/10.1016/j.electacta.2012.02.097

[24] Z. Hu, J. Cai, G. Song, Y. Tian, M. Zhou, Anodic oxidation of organic pollutants: anode fabrication, process hybrid and environmental applications, Curr. Opin. Electrochem. 26 (2021) 100659, https://doi.org/10.1016/j.coelec.2020.100659

[25] S.O. Ganiyu, N. Oturan, S. Raffy, M. Cretin, R. Esmilaire, E. van Hullebusch, G. Esposito, M.A. Oturan, Sub-stoichiometric titanium oxide (Ti4O7) as a suitable ceramic anode for electrooxidation of organic pollutants: a case study of kinetics, mineralization and toxicity assessment of amoxicillin, Water Res. 106 (2016) 171–182, https://doi.org/10.1016/j.watres.2016.09.056

[26] J. Carrillo-Abad, J. Mora-Gómez, M. García-Gabaldón, S. Mestre, V. Pérez-Herranz, Comparison between an electrochemical reactor with and without membrane for the nor oxidation using novel ceramic electrodes, J. Environ. Manag. 268 (2020) 110710, https://doi.org/10.1016/j.jenvman.2020.110710

[27] J. Mora-Gómez, M. García-Gabaldón, J. Carrillo-Abad, M.T. Montañés, S. Mestre, V. Pérez-Herranz, Influence of the reactor configuration and the supporting electrolyte concentration on the electrochemical oxidation of Atenolol using BDD and SnO_2 ceramic electrodes, Sep. Purif. Technol. 241 (2020) 116684, https://doi.org/10.1016/j.seppur.2020.116684

[28] M.I.A.A. Maksoud, G.S. El-Sayyad, A.H. Ashour, A.I. El-Batal, M.A. Elsayed, M. Gobara, A.M. El-Khawaga, E.K. Abdel-Khalek, M.M. El-Okr, Antibacterial, antibiofilm, and photocatalytic activities of metals-substituted spinel cobalt ferrite nanoparticles, Microb. Pathog. 127 (2019) 144–158, https://doi.org/10.1016/j.micpath.2018.11.045

[29] M. Madhukara Naik, H.S. Bhojya Naik, G. Nagaraju, M. Vinuth, H. Raja Naika, K. Vinu, Green synthesis of zinc ferrite nanoparticles in Limonia acidissima juice: characterization and their application as photocatalytic and antibacterial activities, Microchem. J. 146 (2019) 1227–1235, https://doi.org/10.1016/j.microc.2019.02.059

[30] P. Roonasi, A.Y. Nezhad, A comparative study of a series of ferrite nanoparticles as heterogeneous catalysts for phenol removal at neutral pH, Mater. Chem. Phys. 172 (2016) 143–149, https://doi.org/10.1016/j.matchemphys.2016.01.054

[31] A. Behera, D. Kandi, S. Mansingh, S. Martha, K. Parida, Facile synthesis of $ZnFe_2O_4$@RGO nanocomposites towards photocatalytic ciprofloxacin degradation and H_2 energy production, J. Colloid Interface Sci. 556 (2019) 667–679, https://doi.org/10.1016/j.jcis.2019.08.109

[32] N. Matinise, K. Kaviyarasu, N. Mongwaketsi, S. Khamlich, L. Kotsedi, N. Mayedwa, M. Maaza, Green synthesis of novel zinc iron oxide (ZnFe2O4) nanocomposite via Moringa oleifera natural extract for electrochemical applications, Appl. Surf. Sci. 446 (2018) 66–73, https://doi.org/10.1016/j.apsusc.2018.02.187

[33] R. Yang, Y. Ji, J. Zhang, R. Zhang, F. Liu, Y. Chen, L. Liang, S. Han, X. Yu, H. Liu, Efficiently degradation of polyacrylamide pollution using a full spectrum Sn3O4 nanosheet/Ni foam heterostructure photoelectrocatalyst, Catal. Today 335 (2019) 520–526, https://doi.org/10.1016/j.cattod.2019.02.019

[34] R. Daghrir, P. Drogui, D. Robert, Photoelectrocatalytic technologies for environmental applications, J. Photochem. Photobiol. A Chem. 238 (2012) 41–52, https://doi.org/10.1016/j.jphotochem.2012.04.009

[35] Y. Fan Su, G.B. Wang, D.T.F. Kuo, M. ling Chang, Y. Hsin Shih, Photoelectrocatalytic degradation of the antibiotic sulfamethoxazole using TiO_2/Ti photoanode, Appl. Catal. B Environ. 186 (2016) 184–192, https://doi.org/10.1016/j.apcatb.2016.01.003

[36] J. Mora-Gómez, M. García-Gabaldón, E. Ortega, M.J. Sánchez-Rivera, S. Mestre, V. Pérez-Herranz, Evaluation of new ceramic electrodes based on Sb-doped SnO2 for the removal of emerging compounds present in wastewater, Ceram. Int. 44 (2018) 2216–2222, https://doi.org/10.1016/j.ceramint.2017.10.178

[37] J. Gilabert, M.D. Palacios, V. Sanz, S. Mestre, Solution combustion synthesis of $(Co,Ni)Cr_2O_4$ pigments: influence of initial solution concentration, Ceram. Int. 43 (2017) 10032–10040, https://doi.org/10.1016/j.ceramint.2017.05.019

[38] J. Gilabert, M.D. Palacios, M.J. Orts, S. Mestre, Solution combustion synthesis of $(Ni,Fe)Cr_2O_4$ pigments: effect of post-synthesis thermal treatments, Ceram. Int. 43 (2017) 12789–12798, https://doi.org/10.1016/j.ceramint.2017.06.168

[39] K.C. Patil, M.S. Hegde, T. Rattan, S.T. Aruna, Chemistry of nanocrystalline oxide, Materials (2008), https://doi.org/10.1142/6754

[40] D.A.C. Coledam, J.M. Aquino, B.F. Silva, A.J. Silva, R.C. Rocha-Filho, Electrochemical mineralization of norfloxacin using distinct boron-doped diamond anodes in a filter-press reactor, with investigations of toxicity and oxidation by-products, Electrochim. Acta 213 (2016) 856–864, https://doi.org/10.1016/j.electacta.2016.08.003

[41] D.A.C. Coledam, M.M.S. Pupo, B.F. Silva, A.J. Silva, K.I.B. Eguiluz, G.R. Salazar-Banda, J.M. Aquino, Electrochemical mineralization of cephalexin using a conductive diamond anode: a mechanistic and toxicity investigation, Chemosphere 168 (2017) 638–647, https://doi.org/10.1016/j.chemosphere.2016.11.013

[42] A. El-Ghenymy, C. Arias, P.L. Cabot, F. Centellas, J.A. Garrido, R.M. Rodríguez, E. Brillas, Electrochemical incineration of sulfanilic acid at a boron-doped diamond anode, Chemosphere 87 (2012) 1126–1133, https://doi.org/10.1016/j.chemosphere.2012.02.006

[43] A. Özcan, Y. Şahin, A.S. Koparal, M.A. Oturan, Propham mineralization in aqueous medium by anodic oxidation using boron-doped diamond anode: Influence of experimental parameters on degradation kinetics and mineralization efficiency, Water Res. 42 (2008) 2889–2898, https://doi.org/10.1016/j.watres.2008.02.027

[44] I. Sirés, N. Oturan, M.A. Oturan, Electrochemical degradation of β-blockers. Studies on single and multicomponent synthetic aqueous solutions, Water Res. 44 (2010) 3109–3120, https://doi.org/10.1016/j.watres.2010.03.005

[45] D.A.C. Coledam, I. Sánchez-Montes, B.F. Silva, J.M. Aquino, On the performance of HOCl/Fe^{2+}, HOCl/Fe^{2+}/UVA, and HOCl/UVC processes using in situ electrogenerated active chlorine to mineralize the herbicide picloram, Appl. Catal. B Environ. 227 (2018) 170–177, https://doi.org/10.1016/j.apcatb.2017.12.072

[46] S.W. da Silva, E.M.O. Navarro, M.A.S. Rodrigues, A.M. Bernardes, V. Pérez-Herranz, The role of the anode material and water matrix in the electrochemical oxidation of norfloxacin, Chemosphere 210 (2018) 615–623, https://doi.org/10.1016/j.chemosphere.2018.07.057

[47] S.S. Kumbhar, M.A. Mahadik, S.S. Shinde, K.Y. Rajpure, C.H. Bhosale, Fabrication of $ZnFe_2O_4$ films and its application in photoelectrocatalytic degradation of salicylic acid, J. Photochem. Photobiol. B Biol. 142 (2015) 118–123, https://doi.org/10.1016/j.jphotobiol.2014.12.002

[48] N.G. Yadav, L.S. Chaudhary, P.A. Sakhare, T.D. Dongale, P.S. Patil, A.D. Sheikh, Impact of collected sunlight on ZnFe2O4 nanoparticles for photocatalytic application, J. Colloid Interface Sci. 527 (2018) 289–297, https://doi.org/10.1016/j.jcis.2018.05.051

[49] A. Šutka, R. Pärna, J. Kleperis, T. Käämbre, I. Pavlovska, V. Korsaks, K. Malnieks, L. Grinberga, V. Kisand, Photocatalytic activity of non-stoichiometric ZnFe2O4 under visible light irradiation, Phys. Scr. 89 (2014), https://doi.org/10.1088/0031-8949/89/04/044011

[50] M. Shahid, Fabrication of magnesium substituted cadmium ferrite nanoparticles decorated Graphene-Sheets with improved photocatalytic activity under visible light irradiation, Ceram. Int. 46 (2020) 10861–10870, https://doi.org/10.1016/j.ceramint.2020.01.098

[51] E.Z. Hegazy, S.A. Kosa, I.H. Abd Elmaksod, J.T. Mojamami, Preparation, characterization and photocatalytic evaluation of aluminum-doped metal ferrites, Ceram. Int. 45 (2019) 7318–7327, https://doi.org/10.1016/j.ceramint.2019.01.015

[52] H.M. Gobara, I.M. Nassar, A.M.A. el Naggar, G. Eshaq, Nanocrystalline spinel ferrite for an enriched production of hydrogen through a solar energy stimulated water splitting process, Energy 118 (2017) 1234–1242, https://doi.org/10.1016/j.energy.2016.11.001

[53] T.C. Ion, X.C. Structure, R. Faggiani, R.J. Gillespie, J.E. Vekris, The Cadmium(1) Ion, Cd22+; X-Ray crystal structure of Cd2(AICLJ2, 576, (1986), 8–9.

[54] D.L. Reger, S.S. Mason, A.L. Rheingold, Syntheses of the first molecular complexes containing a cadmium-cadmium bond and a cadmium-hydrogen bond, J. Am. Chem. Soc. 115 (1993) 10406–10407, https://doi.org/10.1021/ja00075a085

[55] M.M. Khalaf, H.M. Abd El-Lateef, A.O. Alnajjar, I.M.A. Mohamed, A facile chemical synthesis of $CuxNi(1-x)Fe_2O_4$ nanoparticles as a nonprecious ferrite material for electrocatalytic oxidation of acetaldehyde, Sci. Rep. 10 (2020) 1–14, https://doi.org/10.1038/s41598-020-59655-3

[56] J.D. Corbett, W.J. Burkhard, L.F. Druding, Stabilization of the Cadmium(I) oxidation state. The system Cd-$Cd_2^{I}(AlCl_4)_2$-$Cd^{2}(AlCl_4)_2$, J. Am. Chem. Soc. 83 (1961) 76–80, https://doi.org/10.1021/ja01462a016
[57] D.A. Hames, JamesA. Plambeck, Electrochemistry of zinc, cadmium, and mercury ions in fused $AlCl_3$–NaCl–KCl eutectic, Can. J. Chem. 46 (1968) 1727–1733, https://doi.org/10.1139/v68-287
[58] J. Carrillo-Abad, J. Mora-Gómez, M. García-Gabaldón, E. Ortega, S. Mestre, V. Pérez-Herranz, Effect of the CuO addition on a Sb-doped SnO2 ceramic electrode applied to the removal of Norfloxacin in chloride media by electro-oxidation, Chemosphere 249 (2020) 126178, https://doi.org/10.1016/j.chemosphere.2020.126178
[59] J. Mora-Gomez, E. Ortega, S. Mestre, V. Pérez-Herranz, M. García-Gabaldón, Electrochemical degradation of norfloxacin using BDD and new Sb-doped SnO_2 ceramic anodes in an electrochemical reactor in the presence and absence of a cation-exchange membrane, Sep. Purif. Technol. 208 (2019) 68–75, https://doi.org/10.1016/J.SEPPUR.2018.05.017